RSC Advances

ROYAL SOCIETY OF CHEMISTRY

www.rsc.org/advances

Synthesis of shape controllable cobalt nanoparticles and the shape dependent performance in glycerol hydrogenolysis

Qiying Liu[1,*], Xiaofeng Cao[2,3], Tiejun Wang[1], Chenguang Wang[1], Qi Zhang[1] and Longlong Ma[1]

[1]CAS Key Laboratory of Renewable Energy, Guangzhou Institute of Energy Conversion, Chinese Academy of Sciences, Guangzhou, 510640, P. R. China; [2] State Key Laboratory of Coal Conversion, Institute of Coal Chemistry, Chinese Academy of Sciences, Taiyuan, 030001, P.R. China and [3] University of Chinese Academy of Sciences, Beijing 100049, P.R. China

Cobalt nanorods were synthesized in polyol with using Ir as the nucleation agent and sodium stearate as the surfactant. The aspect ratio of rods can be facilely mediated by Ir/Co molar ratios. During rod growth, the solid cobalt alkoxide and stearate intermediates formed at initial stages and acted as the reservoir to control Co^{2+} reduction, followed by further mediating the rod growth. Stearate played the critical role in controlling the formation of rods by its selective and covalent coating on {10-10} planes, which induces the anisotropic growth through [0002] direction. The cobalt rods presented hcp phase in the center part and fcc phase in the conical tips because of growth rate difference in stages, showing the hybrid crystallographic property. The slow growth can also induce the formation of fcc spheres by altering the alkali amount in polyol. In glycerol hydrogenolysis, the hcp rods with the mainly exposed {10-10} planes revealed much higher activity and 1,3-propanediol selectivity than the fcc spheres, demonstrating the facet-dependent performance as solid catalyst. To our knowledge, this is the first example for producing 1,3-propanediol by using facet effect of cobalt nanomaterials.

Key words: Cobalt nanorods, heterogeneous nucleation, growth mechanism, glycerol hydrogenolysis, 1,3-propanediol

Corresponding author:

Qiying Liu, Tel: +86-20-87048614, Fax: +86-20-87057789, E-mail: liuqy@ms.giec.ac.cn.

1 Introduction

Nano-metal materials with different sizes and shapes showed recently the significant applications in catalysis, selective sensing and optical performance.[1-4] Among those, cobalt nanomaterials with well defined geometries gained considerable attention owing to its applications in high density data storage[5], magnetic separation[6] and heterogeneous catalysis[7,8]. Generally, these cobalt nanomaterials possess different crystallographic planes and relatively discrete energy band, both of which show the distinct ability to absorb/activate reactant molecule and mediate their catalytic performance. On the other hand, the shape of cobalt nanomaterials presents orientation effect along exotic magnetic field, thus altering the magnetic properties. Comparing to the spherical nanoparticles, the one-dimensional cobalt nanowires showed the significantly enhanced magnetic performance with larger coercivity and higher blocking temperature.[9] Interestingly, the cobalt nanoparticles with larger sizes possessed higher activity and C_{5+} hydrocarbons selectivity in Fischer-Tropsch Synthesis.[10] Moreover, due to the mainly exposed {100} planes of cobalt nanocubes, the activity was comparable to the spherical cobalt which is mainly exposed {111} planes, but the selectivity for C_{10+} hydrocarbons was much higher than the latter one, demonstrating the facet-dependent catalytic performance.[11,12]

Large numbers of strategies were employed to synthesize cobalt nanomaterials with well defined geometries. By using ordered mesoporous SiO_2, ZrO_2, carbon nanotube, polystyrene as the hard templates,[13-16] and polyvinylpyrrolidone (PVP), cetyl trimethylammonium bromide (CTAB), sodium dodecyl sulfonate (SDS) as the soft templates,[17-19] cobalt nanowires, nanocubes and hollow spheres can be synthesized. In the presence of surfactants, cobalt nanorods/wires, discs and spherical nanocrystallines were also fabricated via thermal pyrolysis of cobalt contained precursors in organic solvents[20,21] and reverse micro-emulsion systems[22]. However, these cobalt nanosmaterials obtained need multi-steps for hard/soft template, cost/toxic organometallic precursors for thermal pyrolysis, and complex reaction medium for reverse micro-emulsion. Comparatively, polyols are effective for synthesizing metal nanomaterials as solvent, reductant and complexant.[23,24] However, due to the mild reducing

capability of polyol and negative redox potential of cobalt cation, the synthetic temperature is rather high (the reduction usually takes place at the boiling point of polyol), which results in exquisite shape and particle size control of cobalt nanomaterials rather difficult.[25] A solution is to introduce exotic nucleus to facilitate cobalt nucleation at lower temperature for preferring the relatively separated nucleation and growth process and mediating the shape and size of metal nanomaterials.[26,27]

In this work, we solvothermally fabricate cobalt nanorods with controllable aspect ratios and nanospheres with difference sizes by selecting Ir as the heterogeneous nucleation agent in 1,2-propanediol and sodium stearate. The structure of nanorods/nanospheres was elucidated and the formation mechanism was proposed. These nanoparticles were used as the catalyst for selective hydrogenolysis of glycerol to 1,2-/1,3-propanediols and the interesting facet-dependent catalysis was obtained.

2 Experimental section

2.1 Materials synthesis

The cobalt nanomaterials were synthesized by a typical solvothermal process. 0.75 g cobalt acetate tetrahydrate and a certain amount of NaOH were mixed and dissolved in 70 ml 1,2-propanediol to obtain a purple solution under stirring and mild heating. A given amount of sodium stearate and $H_2IrCl_6.6H_2O$ dissolved in 5 ml 1,2-propanediol were then added to obtain a blue flocculent solution and continue stirring for several minutes. The flocculent solution was transferred to a 100 ml autoclave line with Teflon and sealed, followed by gradually heating to 150 ℃. After maintaining for a certain time, the autoclave was cooled to ambient temperature. The black solid was centrifuged, thoroughly washed with ethanol and deionized water, and finally dried under vacuum at 60 □ for 5 h.

2.2 Materials characterization

The Powder X-ray diffraction (XRD) patterns were recorded on a diffractometer (XPert Pro MPD, Philip) operated at 40 kV and 100 mA by using nickel-filtered Cu K_α radiation (λ=1.5418 Å), and the low angle XRD pattern was

obtained on the same instrument with the exception of the operating current 30 mA.

Transmission electron microscope (TEM) and high resolution transmission electron microscope (HRTEM) images were taken using a JEOL JEM-2100F instrument operated at 200 kV. The samples were ultrasonically dispersed into ethanol, and drops of the suspension were placed on a carbon-coating copper grid and then dried in air.

SEM images of cobalt materials were recorded using an S-4800 instrument operated at 30 kV. The sample was placed on a conductive carbon tape adhered to an aluminum sample holder.

The elemental analyses were performed by Inductively Coupled Plasma Atomic Emission Spectroscopy (ICP-AES) on a Plasma-Spec- spectrometer (LEEMAN, USA). The samples were dissolved into aqua regia, and the solution was diluted with 2% HNO_3 to meet the detect range of the instrument.

The N_2 adsorption-desorption isothermal profile was performed on a Micromeritics ASAP 2010 system at -196 . Before measurement, the samples were degassed under vacuum for 6 h at 80 . The surface area was calculated by the multipoint Braunauer-Emmett-Teller method.

The FT-IR spectra were obtained in the scanning range of 4000-400 cm^{-1} by using a Nicolet 6700 FT-IR spectrometer with a resolution of 4 cm^{-1}. The sample was fully grinded with KBr and pressed into wafer before measurement.

The TG curves were conducted on a NETZSCH-STA 409PC DSC-SP thermal analyzer under the N_2 flow of 30 ml/min with a ramp of 10 /min from room temperature to 630 .

The XPS measurements were performed with a Surface Science Instruments SSX-100 ESCA spectrometer using monochromatic Al K_α X-rays and an electrostatic hemispherical analyzer. The spectra were recorded with a pass energy of 110 eV and an X-ray spot size of 600 μm. The base pressure in the analysis chamber was around 10^{-9} Torr. A flood gun type charge neutralizer was used to correct for differential charging. For XPS measurements, the samples were pretreated at 100 ℃ in a reactor cell under N_2 flow and then transferred under vacuum to the analysis chamber.

2.3 Glycerol hydrogenolysis

Hydrogenolysis of glycerol was carried out in a 100 ml autoclave with a mechanical stirring. 0.06 g cobalt nanomaterials were added to 40 g aqueous solution of 10 wt % glycerol. After removing the residue air in autoclave by H_2 flush, the reactor was pressurized to 3.0 MPa. The reaction system was heated to 200 ℃ and kept at the temperature for a certain period under vigorous stirring. After reaction, the system was cooled in ice water. For evaluating the catalytic stability, the cobalt nanomaterials were collected after each run, washed with deionized water and reused directly for the next cycle. As a reference, Ir was used as the catalyst for this reaction. 0.0015 g $H_2IrCl_6.6H_2O$ (the Ir amount was calculated as the stoichiometric ones comprised in 0.06 g cobalt) dissolved in 40 ml water was reduced in the same reactor under H_2 at 250 □ for 0.5 h. After cooling to room temperature in ice water, 4 g glycerol was introduced into the black colloidal solution and the hydrogenolysis procedure was the same to those mentioned above.

The liquid products were identified by GC-MS and quantified by a gas chromatography (Agilent 7890) equipped with a flame-ionization detector and a Carbowax 20 M capillary column with 25 m in length and 0.2 mm in diameter. 1,4-Butanediol was used as the internal standard. The gas products were collected by a gas bag and were analyzed by a another gas chromatography equipped with a thermal conductivity detector and a Porapak-T (3 m×3 mm) pack column.

Glycerol conversion and product selectivity are defined as the following formulas:

$$\text{Glycerol conversion} = \frac{C^{o}_{Glycerol} - C_{Glycerol}}{C^{o}_{Glycerol}} \times 100\% \quad (C_{Glycerol} = \frac{(a_{Glycerol} + b_{Glycerol} A_{Glycerol} A_S^{-1}) W_s}{W_{Solution}}).$$

$$\text{Product selectivity (C-mol\%)} = \frac{92 m_i C_i M_i^{-1}}{3(C^{o}_{Glycerol} - C_{Glycerol})} \times 100\% \quad (C_i = \frac{(a_i + b_i A_i A_S^{-1}) W_S}{W_{Solution}}).$$

Here, *C, W, A and M* refer to mass concentration, weight, peak area (in gas chromatography analysis) and molecular weight of weight of glycerol and product, respectively. The subscript *i* and *s* mean product *i* and the internal standard *s*. m_i indicates carbon numbers of product *i,* and *a* and *b* are the parameters of product *i* in correction curves during quantification analysis.

3 Results and discussion

3.1 Shape control of cobalt materials

Figure 1 shows the influence of Ir/Co molar ratios on cobalt shape. Without Ir, the cobalt was spheres with the diameter of about 500 nm. At the Ir/Co molar ratio of 0.01, the spheres disappeared and the cobalt nanorods with the length of 100-300 nm and the diameter of about 10 nm were observed instead. On each rod terminal, the conical head of about 30 nm was observed. As the Ir/Co was increased to 0.025, the rod like shape was preserved, but the length was decreased to 50-200 nm and the conical heads were absent in this case. As the Ir/Co ratio was further increased to 0.05, the rod diameter changed a litter but the length continuously decreased to about 40 nm.

The structural details of rods were characterized by HRTEM. As shown in Figure 2a, the consistent lattice fringes of 0.211 nm, 0.208 nm and 0.188 nm are corresponded to the (10-10), (0002) and (10-11) planes, respectively, indicating the hexagonal close-packed phase of metal cobalt (hcp, JCPDS No. 5-727). Based on Figure 2a and the FFT pattern, the rods grow along [001] plane and the mainly exposed planes are the enclosed {1010} at the lateral directions. The structure of conical head was revealed in Figure 2b and d. Along the [0002] direction of nanorods, the conical heads presented as the regular hexagon and the average size was about 28 nm with the side length of about 15 nm, which is well consistent with the size measurement by TEM (Figure 1b). Interestingly, the HRTEM measurement and relative FFT pattern showed that the distinct lattice fringes of 0.203 nm are relative to the (111) plane of face-centered cubic phase of metal cobalt (fcc, JCPDS No. 15-806). These fringes are perpendicular to the long axis of nanorods, revealing the mainly exposed (111) plane. Evidently, the crystallography of the synthetic cobalt nanorods is composed of hcp phase in centered part and fcc phase in conical tips.

Besides the rods, multi-pods nanostructures with three, four and five branches were observed in the cases of the Ir/Co molar ratios being 0.01 and 0.025 (Figure 3). The length of each branch varied in 30-200 nm but their diameter was the similar 10 nm to the isolate rods. In some cases, the branches extruded out from a bending or a straight rod substrate, forming the quasi-tetrapod structure.

Figure 4 shows the XRD patterns of cobalt nanomaterials synthesized with different Ir/Co molar ratios. When no Ir was introduced and the synthesis was lasted for 20 h, the diffractions at 2θ= 44.4 °, 51.6 ° and 76 ° are relative to the (111), (200) and (220) planes, respectively, indicating the fcc phase of the cobalt spheres. As Ir was added and the synthesis was implemented for 10 h, the fcc phase was disappeared. The distinct diffractions at 2θ= 41.5 °, 44.4 °, 47.4 °, 62.4 ° and 75.9 ° are corresponding to the (10-10), (0002), (10-11), (10-12) and (1100) planes, respectively, demonstrating that the crystallography of cobalt is hcp phase. The relative (0002) diffraction significantly intensified with increasing the Ir/Co molar ratio, indicating the preferential orientation of the rods. According to Scherrer equation, we calculated the consistent diffraction length based on the (10-10) and (0002) planes in Figure 4d. The lengths along the [10-10] and [0002] directions were 12 nm and 43 nm, respectively, which is well consistent with the TEM measurements (Figure 1d and Figure 2a).

The influence of NaOH on the cobalt morphology was shown in Figure 5. Without alkali, the cobalt was spherical and the size was about 30 nm. These nanospheres aggregated into the large particles of 100-300 nm, followed by further self-assembly into the one-dimensional chain structure. As the appropriate NaOH of 0.2 g was used, the chain like structure was transferred into the nanorods with the length of 50-200 nm and the diameter of about 10 nm. However, as the NaOH amount was further increased to 0.7 g, the cobalt shape changed back to the spheres of 100-200 nm with a rough surface. Based on the previous reports, the spheres synthesized at high basicity were possibly ascribed to the slow growth of cobalt materials.[28,29]

Figure 6 shows the XRD patterns of the cobalt nanomaterials synthesized with different NaOH amounts. When no NaOH was used, the crystallographic phase of the small spheres was the pure fcc structure. As expected, the cobalt nanorods presented as the pure hcp phase at the NaOH amount of 0.2 g. When the NaOH was further increased to 0.7 g, the mixed hcp and fcc phases were obtained. The significantly intensified diffraction at 2 θ=44.4 ° is attribute to the superimposition of the hcp (0002) and fcc (111) planes of cobalt.[28] Based on the previous report, we confirmed that the

relative content of fcc phase was about 65%.[29]

3.2 Formation mechanism of cobalt materials

To ascertain the growth mechanism of cobalt nanorods, the samples at different time were collected during synthesis and their respective shape and the crystallographic phase evolution were monitored by TEM and XRD measurements (Figure 7 and 8). At 0.5 h, the solid recovered was purple and presented as several hundred nanometers with significant aggregation. Its diffractions below 30 ° indicated the mixed phase of cobalt stearate and cobalt alkoxide.[30,31] No diffraction relative to metallic cobalt was observed, implying only solid cobalt precursors form at this stage. The two solid intermediates were produced via the reaction of dissolved Co^{2+} with stearate and 1,2-propanediol in the presence of alkali, as indicated by our and other previous reports. From the diffraction intensities, cobalt stearate seems as the major one perhaps due to that the more electronegative of carboxyl groups in stearate could easily capture the dissolved Co^{2+} to form the cobalt stearate precipitate. The low angle XRD pattern of the solid intermediates displayed four distinct diffractions at 2θ=1.82 °, 3.64 °, 5.44 ° and 7.25 °, which is responsible for the respective (001), (002), (003) and (004) facets of laminated cobalt stearate. By using the primary (001) facet, we confirmed that the interlayer space was 4.85 nm. Considering the aliphatic chain length of 2.5 nm in stearate, this distance is about two times of a single chain length, indicating the bi-layered structure of cobalt stearate.[32]

As the time prolonging to 1 h, the TEM image proposed the formation of mixed particles and rods with the particles as the majority, apart from the solid intermediates. The particle size was in the range of 5-20 nm while the rod diameter and length were about 7 nm and 50-100 nm, respectively, which demonstrates Co^{2+} starts to be reduced at this stage. The formation of large particles was possibly ascribed to the continuous growth during cooling because such size can't grow into the rods with the diameter of 10 nm. With the time increasing to 1.5 h, the particles grew into the nanorods at the expense of the cobalt contained intermediates. The XRD pattern showed that no other diffractions were observed but a very weak one at 2θ=20 °, indicating the crystallized intermediates transferred to amorphous matter owing to

consumption. Instead, the hcp cobalt phase was seen by weak diffractions. When the time was increased to 10 h, the rods continued growing to obtain the length of 200 nm while with the diameter slightly rising to about 10 nm. During this process, the diffraction of hcp cobalt gradually intensified accompanied with the solid intermediates reduced until complete consumption. Similarly, the conical tips on one terminal rod at early stages are possibly due to the same reason for the formation of large particles at 1 h.

During synthesis, the solid intermediates cobalt stearate and alkoxide decrease the dissolved Co^{2+} concentration in 1,2-propanediol as Co^{2+} reservoir and decrease the supersaturation of Co^{2+} by controlling Co^{2+} release into the solution. Here, H_2IrCl_6 is simultaneously introduced with cobalt acetate. Due to its higher redox potential than Co^{2+}, the Ir^{4+} ions can be first and fast reduce to nanoparitcles by 1,2-propanediol. As heterogeneous nucleation agent, the tiny Ir particles facilitate the Co^{2+} reduction to nanocrystals by the same solvent, followed by growing into rods. With regarding to the absence of Ir particles in XRD patterns (Figure 4, 6 and 8)), we measured the content of Ir residue on cobalt nanomaterials by means of ICP-AES. As shown in Table 1, the Ir/Co molar ratios in the final rods and spheres were much lower than the initially introduced counterparts, indicating that most Ir particles were removed during washing procedure. Occasionally, the isolated 2-3 nm Ir particles were observed by HRTEM measurement (Figure 2c).

In the presence of exotic Ir as the nucleation agent, the reduction of dissolved Co^{2+} is accelerated and thus induces a relatively separated nucleation and growth process,[33] which is favorable for the fast growth of nanocrystals into rods. For the formation of cobalt nanorods, the length is determined by the Co amount for growth. At high Ir/Co ratio, more Ir particles induce more Co nucleus explosion at nucleation stage, which leads to less cobalt atoms for subsequential growth and finally obtained the rods with low aspect ratios (Figure 1). In some cases, the conical tips with large size were observed. Based on the previous reports, its formation is perhaps attribute to the slow growth at final stage where the Co^{2+} concentration in solution is very low.[34,35] This slow growth results in the stacking model of reduced cobalt atoms via the ABCABC… sequence along [111] direction of fcc phase, which is very different from the ABAB…

sequence along the [0002] orientation of hcp cobalt phase under fast growth.[36] The both factors dominate the formation of rods having the hybrid hcp and fcc phases.

Based on Figure 5 and 6, the hcp cobalt nanorods can be synthesized at the medium basicity because the low and high basicities lead to the formation of fcc spheres and mixed fcc/hcp spheres, respectively. As proposed by the previous reports, H^+ is produced by dehydrogenation and accumulated during Co^{2+} reduction by 1,2-propanediol.[37,38] The addition of appropriate NaOH can counteract H^+ and push the reaction proceeds, thus accelerating cobalt growth into the rods. Vice versa, the formation of spheres is owing to the low growth of cobalt.

In addition to the isolated rods, a significant amount of multi-pods with isotropic and unisotropic geometries were obtained at the appropriate Ir/Co ratios (Figure 3). At early stage, the tiny cobalt nanocrystals with specific facets of high energy could form. These facets possibly serve as the seeds for epitaxial stacking of reduced cobalt atoms from three dimensions to form the final isotropic multi-pods.[39] During fast growth of rod, the stacking faults easily form.[40] These faults are high energy and favorable for capturing cobalt atoms to gain the second seeds, followed by growth into the branched rods from the substrate to get the unisotropic multi-pods. This hypothesis was evidenced by the fact that the extrusions were unambiguously observed on some rods (Figure 3d, as labeled by the circles) and survived from rod synthesis.

Surfactant is widely used for synthesizing well-defined metal nanostructures via its selective capping effect.[41] Here, the employed sodium stearate is critical for cobalt nanorods and multi-pods. In hcp cobalt, the surface energy of lateral {10-10} facets is higher than those of the axial {0002} ones.[42] This induces the selective capping of stearate on them and mediates the rods growing along the [0002] orientation. Figure 9 shows the FT-IR spectra of cobalt nanorods synthesized at different time. For the pure sodium stearate, the peaks observed were relative to the stretching vibrations of aliphatic C-H (2950-2850 cm^{-1}) and carboxyl group ($-COO^-$, 1566 cm^{-1} and 1428 cm^{-1}), and the scissoring vibration of C-H (1468 cm^{-1}).[32] As the time prolonged, the absorbencies decreased but were still observed at the end 10 h,

indicating that the cobalt stearate decompose due to Co^{2+} reduction and release the excessive stearate into solution, remaining the minority capping on cobalt rod surface. We confirmed the amount of capping stearate on the rods synthesized at 10 h by TG analysis. As shown in Figure 10, the about 2% of weight loss before 150 ℃ is ascribed to the removal of physically absorbed water. The second loss at 295 ℃ is about 14%, indicating the thermal decomposition of stearate. We used XPS to analyze the chemical status of stearate with different aspect ratios (Figure 11). The Co 2p doublet at the binding energies of 779.1 eV and 794.5 eV indicated the mixed Co and $Co^{\delta+}$ species combined with carboxylate.[42] This combination is demonstrated by the binding energy of C 1s at 289.4 eV (C-O bond). The other C 1s peak at 284.8 eV is responsible for the carbons in aliphatic chain (C-C bond) in stearate. As carboxylic acid absorbs on metal surface, two bonding types, including the monodentate bond with inequivalent oxygen atom or the bidentate bond with equivalent oxygen atom, are proposed.[43] If the monodentate bond takes place, the O 1s peak corresponding to C=O would be observed at the binding energy of about 533 eV. However, our result shows that only one peak is presented at 530.5 eV (C-O bond), indicating the bonding model for stearate is bidentate.

3.3 Catalytic Performance of cobalt materials

Glycerol is the byproduct of biodiesel synthesis by transesterification of vegetable oil and methanol.[44] Converting glycerol into value-added chemicals can improve the comprehensive benefit. A promising route is to selective glycerol hydrogenolysis to 1,2-/1,3-propanediols which widely used in fine, organic and medicine chemical industries as the feedstock and/or intermediate. The catalysts for this process mainly depend on the supported noble metals Ru, Rh, Pt, Pd and transition metals Cu and Ni.[45,46] Over this kind of catalyst, the main product is 1,2-propanediol. To produce more valuable 1,3-propanediol, the medium hydroxyl group needs to be removed. However, due to the steric blockage the removal of medium hydroxyl group is rather difficult. When using Pt, Ir aided by WO_x, ReO_x, AlO_x as the catalyst, 1,3-propanediol can be produced with the yields.[47,48] Cobalt platelets and polyhedrons were recently used for glycerol hydrogenolysis, but only 16% of 1,2-propanediol yield was obtained.[49]

Here, we used cobalt nanorods and spheres for this process. The detectable and identified products contain 1,2-/1,3-propanediols, acetol, 1-propanol, ethylene glycol and ethanol. Considering Ir was reported as the active metal, we prepared the equivalent Ir particles according to the Ir residue on cobalt rod surface and implemented the comparison experiment under the same condition. The result showed that the glycerol conversion was lower than 3%, indicating its catalytic performance can be ruled out. As shown in Table 2, the nanorods showed more than 60% of glycerol conversion with the total 1,2-/1,3-propanediols selectivity of more than 65%, and the highest propanediols yield of 59% was obtained over the rods (Figure 1b) having the largest surface (Table 1). Comparatively, the spheres showed much lower activities than the rods. Besides activity, the rods presented the remarkably higher 1,3-propanediol selectivity and the highest yield of 19% was obtained. The superior performance of rods is dependent on their exposed {10-10} facets, which is favorable for glycerol hydrogenolysis to propanediols due to the higher surface energy than that of the possibly exposed {111} planes on the spheres.[38] Figure 12 compared the activity and 1,3-propanediol productivity on unit surface area of rods and spheres. The respective activity and 1,3-propanediol productivity over the rods were two and ten times higher than those obtained over the spheres. To our knowledge, this is the first example to mediate 1,2- and 1,3-propanediol selectivities in glycerol hydrogenolysis by controlling the morphology of cobalt materials.

Figure 13 shows the influence of reaction time on glycerol hydrogenolysis over cobalt rods and spheres. For the rods, the glycerol conversion increased with increasing reaction time and the maximal 87% was obtained at 16 h. Meanwhile, the 1,2-/1,3-propanediol selectivities presented the volcano feature with the respective maximal 36% and 58% at the time of 5 h, and then reduced to 41% and 24%, respectively, when the duration was lengthened to 16 h. Besides the goal products, acetol which is produced by dehydrated removal of tip hydroxyl in glycerol monotonously decreased with the increased reaction time due to it is further hydrogenated to 1,2-propanediol.[47] The further hydrogenolysis of propanediols resulted in the gradually rise of 1-propanol while with the selectivities below than 10%, indicating this

kind of side product was suppressed. Additionally, ethylene glycol produced by glycerol dehydrogenation followed by retro-aldolation was observed[48] and the selectivities were monotonously increased to about 10%. Over the cobalt rods, we obtained significant amount of 1,3-propanediol in final products. However, we do not detect 3-hydroxy-propanal even at low glycerol conversion, which is possibly attribute to its fast hydrogenation to 1,3-propanediol.[48] As the cobalt spheres were used, the similar phenomena were observed, but the higher 1,2-propanediol and much lower 1,3-propanediol selectivities were gained as comparing to the rods. Over both rods and spheres, the gas phase was analyzed and H_2, CO_2 and CH_4 were detected as the main products, indicating aqueous phase reforming of glycerol and diols/mononic alcohols takes place in our cases.[50]

The catalytic stability of cobalt rods and spheres was revealed in Figure 14. Over the cobalt rods, the glycerol conversion slightly decreased from 80% for the first run to 70% for the third run together with the slightly reduced 1,3-propanediol (from the first 26% to the third 21%) and increased 1,2-propanediol (from the first 49% to the third 58%) selectivities. As the cycle proceed, comparatively, the glycerol conversion significantly decreased from the first 30% to the third 5% over the cobalt spheres despite the 1,3-propanediol and 1,2-propanediol selectivities keeping the constant 5% and 60%, respectively. Obviously, the rods show superior stability to the spheres in glycerol hydrogenolysis.

The TEM images of used cobalt materials were shown in Figure 15. After three cycles, the surface of the rods became rough but the one-dimensional shape was largely kept, indicating the rods in our case are “robust” in this process. By comparison, the spheres were agglomerated severely into several hundred nanometers, showing that the spheres are rather morphologically unstable in the present hydrogenolysis conditions. This aggregation is responsible to the remarkable loss of surface area (Table 1) and is accordingly unreusable in glycerol hydrogenolysis. It’s noted that the retention of the rod like shape and surface area (Table 1) after reuse may propose the main reason for keeping the superior performance to the spheres.

4 Conclusions

Cobalt nanorods were solvothermally fabricated in polyol by using Ir as the exotic nucleation agent and sodium stearate as the surfactant. The shortened rods were obtained at higher Ir/Co molar ratios, which is possibly due to that more Ir nanoparticles induce more cobalt nucleus burst out at initial stage remaining less cobalt atoms for the sequential growth. During rods growth from nanocrystals, cobalt alkoxide and stearate form at early stages and serve as the solid intermediates to control the dynamic Co^{2+} reduction. Stearate plays the essential role in controlling the formation of rods by its selective, covalent capping on the lateral {10-10} planes and mediating the anisotropic growth along [0002] orientation. The rods show the interesting hcp phase in the center part and fcc phase in the conical tips. The fcc tips are produced by the slow growth due to the reduced Co^{2+} concentration at end stage. The slow growth rate also induces the formation of fcc nanospheres by controlling the basicity in solution. In glycerol hydrogenolysis, the hcp rods with mainly exposed {10-10} planes exhibited two times higher activity and ten times higher 1,3-propanediol productivity than the fcc spheres based on unit surface area, showing the interesting facet-dependent catalysis.

Acknowledgements

This work is financially supported by the National Natural Science Foundation of China (51376185), the National Basic Research Program of China (2012CB215304), the Natural Science Foundation of Guangdong Province (S2013010011612 and S20122040006992) and the Creative Foundation of President of Guangzhou Institute of Energy Conversion, Chinese Academy of Sciences (y307p21001).

References

[1] M. T. Zhao, K. Deng, L. C. He, Y. Liu, G. D. Li, H. J. Zhao and Z. Y. Tang, *J. Am. Chem. Soc.*, 2014, **136**, 1738.

[2] L. C. He, Y. Liu, J. Z. Liu, Y. S. Xiong, J. Z. Zheng, Y. L. Liu and Z. Y. Tang, *Angew. Chem. Int. Ed.*, 2013, **52**, 3741.

[3] H. J. Yin, H. J. Tang, D. Wang, Y. Gao and Z. Y. Tang, *ACS Nano*, 2012, **6**, 8288.

[4] J. X. Gong, F. Zhou, Z. Y. Li and Z. Y. Tang, *Chem. Commun.*, 2013, **49**, 4379.

[5] S. Singamaneni, V. N. Bliznyuk, C. Binek and E. Y. Tsymbal, *J. Mater. Chem.*, 2011, **21**, 16819.

[6] H. Zeng and S. H. Sun, *Adv. Funct. Mater.*, 2008, **18**, 391.

[7] Y. Li, Q. Y. Liu and W. J. Shen, *Dalton Transctions*, 2011, **40**, 5811.

[8] V. Polshettiwar, R. Luque, A. Fihri, H. B. Zhu, M. Bouhrara and J. M. Basset, *Chem. Rev.*, 2011, **111**, 3036.

[9] K. A. Atmane, F. Zighem, Y. Soumare, M. Ibrahim, R. Boubekri, T. Maurer, J. Margueritat, J. Y. Piquemal, F. Ott, G. Chaboussant, F. Schoenstein, N. Jouini and G. Viau, *J. Solid State Chem.*, 2013, **197**, 297.

[10] G. L. Bezemer, J. H. Bitter, H. P. C. E. Kuipers, H. Oosterbeek, J. E. Holewijn, X. D. Xu, F. Kapteijn, A. J. van Dillen and K. P. de Jong, *J. Am. Chem. Soc.*, 2006, **128**, 3956.

[11] M. Scariot, D. O. Silva, J. D. Scholten, G. Machado, S. R. Teixeira, M. A. Novak, G. Ebeling and J. Dupont, *Angew. Chem. Int. Ed.*, 2008, **47**, 9075.

[12] D. O. Silva, J. D. Scholten, M. A. Gelesky, S. R. Teixeira, A. C. B. D. Santos, E. F. Souza-Aguiar and J. Dupont, *ChemSusChem*, 2008, **1**, 291.

[13] T. A. Crowley, K. J. Ziegler, D. M. Lyons, D. Erts, H. Olin, M. A. Morris and J. D. Holmes, *Chem. Mater.*, 2003, **15**, 3518.

[14] J. C. Bao, C. Y. Tie, Z. Xu, Q. Ma, J. M. Hong, H. Sang and D. Sheng, *Adv. Mater.*, 2002, **14**, 44.

[15] S. W. Liu, J. J. Zhu, Y. Mastai, I. Felner and A. Gedanke, *Chem. Mater.*, 2000, **12**, 2205-2211.

[16] A. K. Srivastava, S. Madhavi, T. J. White and R. V. Ramanujan, *J. Mater. Chem.*, 2005, **15**, 4424.

[17] L. Guo, F. Liang, N. Wang, D. S. Kong, S. M. Wang, L. He, C. P. Chen, X. M. Meng and Z. Y. Yu, *Chem. Mater.*, 2008, **20**, 5163.

[18] J. Zhang, Z. H. Dai, J. C. Bao, N. Zhang and M. A. López-Quintela, *J. Colloid Interface. Sci.*, 2007, **305**, 339.

[19] J. Huang, L. He, Y. H. Leng, W. Zhang, X. G. Li, C. P. Chen and Y. Liu, *Nanotechnology*, 2007, **18**, 415603.

[20] V. F. Puntes, D. Zanchet, C. K. Erdonmez and A. P. Alivisatos, *J. Am. Chem. Soc.*, 2002, **124**, 12874.

[21] F. Dumestre, B. Chaudret, C. Amiens, M. Respaud, P. Fejes, P. Renaud and P. Zurcher, *Angew. Chem. Int. Ed.*, 2003, **42**, 5213.

[22] I. Lisiecki, M. Walls, D. Parker and M. P. Pileni, *Langmuir*, 2008, **24**, 4295.

[23] M. A. Mahmoud, M. A. El-Sayed, J. P. Gao and U. Landman, *Nano Lett.*, 2013, **13**, 4739.

[24] Y. Q. Zheng, J. Zeng, A. Ruditskiy, M. C. Liu and Y. N. Xia, *Chem. Mater.*, 2014, **26**, 22.

[25] G. V. Kurlyandskaya, S. M. Bhagat, C. Luna and M. Vazquez, *J. Appl. Phys.*, 2006, **99**, 104308.

[26] D. Ung, G. Viau, C. Ricolleau, F. Warmont, P. Gredin and F. Fiévet, *Adv. Mater.*, 2005, **17**, 338.

[27] Y. Soumare, C. Garcia, T. Maurer, G. Chaboussant, F. Ott, F. Fiévet, J. Y. Piquemal and G. Viau, *Adv. Funct. Mater.*, 2009, **19**, 1971.

[28] D. Ung, G. Viau, F. Fiévet-Vincent, F. Herbst, V. Richard and F. Fiévet, *Prog. Solid State Chem.*, 2005, **33**, 137.

[29] P. Toneguzzo, V. Giau, O. Acher, F. Fiévet-Vincent and F. Fiévet, *Adv. Mater.*, 1998, **10**, 1032.

[30] J. M. Rueff, N. Masciocchi, P. Rabu, A. Sironi and A. Skoulios, *Chem. Eur. J.*, 2002, **8**, 1813.

[31] N. Chakroune, G. Viau, C. Ricolleau, F. Fiévet-Vincent and F. Fiévet, *J. Mater. Chem.*, 2003, **13**, 312.

[32] X. Z. Luo, Z. Q. Zhang and Y. Q. Liang, *Langmuir*, 1994, **10**, 3213.

[33] E. A. Aunmol, P. Kundu, P. A. Deshpande, G. Madras and N. Ravishankar, *ACS Nano*, 2011, **5**, 8049.

[34] Q. Y. Liu, X. H. Guo, T. J. Wang, Y. Li and W. J. Shen, *Mater. Lett.*, 2010, **64**, 1271.

[35] M. Ibrahim, C. Marcelot-Garcia, K. A. Atmane, E. Berrichi, L. M. Lacroix, A. Zwick, E. Warot-Fonrose, S. Lachaize, P. Decorse, J. Y. Piquemal and G. Viau, *J. Phys. Chem. C*, 2013, **117**, 15808.

[36] C. Osorio-Cantillo, O. Perales-Perez and M. J. F. Guinel, *J. Appl. Phys.*, 2011, **109**, 07B531.

[37] S. E. Skrabalak, B. J. Wiley, M. Kim, E. V. Formo and Y. N. Xia, *Nano Lett.*, 2008, **8**, 2077.

[38] K. A. Atmane, C. Michel, J. Y. Piquemal, P. Sautet, P. Beaunier, M. Giraud, M. Sicard, S. Nowak, R. Losnoe and G.

Viau, *Nanoscale*, 2014, **6**, 2682.

[39] Y. Dai, X. L, Mu, Y. M. Tan, K. Q. Lin, Z. L. Yang, N. F. Zheng and G. Fu, *J. Am. Chem. Soc.*, 2012, **134**, 7073.

[40] Y. Y. Gao, G. M. Xing, W. G. Chu, X. J. Liang, Y. L. Zhao, L. Jing, H. Yuan, Y. Y. Cui and J. Q. Dong, *Adv. Mater.*, 2008, **20**, 1794.

[41] H. G. Liao, K. Y. Niu and H. M. Zheng, *Chem. Commun.*, 2013, **49**, 11720.

[42] N. Q. Wu, L. Fu, M. Su, M. Aslam, K. C. Wong and V. P. Dravid, *Nano Lett.*, 2004, **4**, 383.

[43] A. Wühn, J. Weckesser and C. Wöll, *Langmuir*, 2001, **17**, 7605.

[44] D. Y. C. Leung, X. Wu and M. K. H. Leung, *Appl. Energy*, 2010, **87**, 1083.

[45] A. M. Ruppert, K. Weinberg and R. Palkovits, *Angew. Chem. Int. Ed.*, 2012, **51**, 2564.

[46] M. A. Dasari, P. P. Kiatsimkul, W. R. Sutterlin and G. J. Suppes, *Applied Catalysis A*, 2005, **281**, 225.

[47] Y. Nakagawa, Y. Shinmi, S. Koso and K. Tomishige, *J. Catal.*, 2010, **272**, 191.

[48] R. Arundhathi, T. Mizugaki, T. Mitsudome, K. Jitsukawa and K. Kaneda, *ChemSusChem*, 2013, **6**, 1345.

[49] Y. B. Cao, X. Zhang, J. M. Fan, P. Hu, L. Y. Bai, H. B. Zhang, F. L. Yuan and Y. F. Chen, *Cryst. Growth Design*, 2011, **11**, 472.

[50] R. D. Cortright, R. R. Davda and J. A. Dumesic, *Nature*, 2002, **418**, 964.

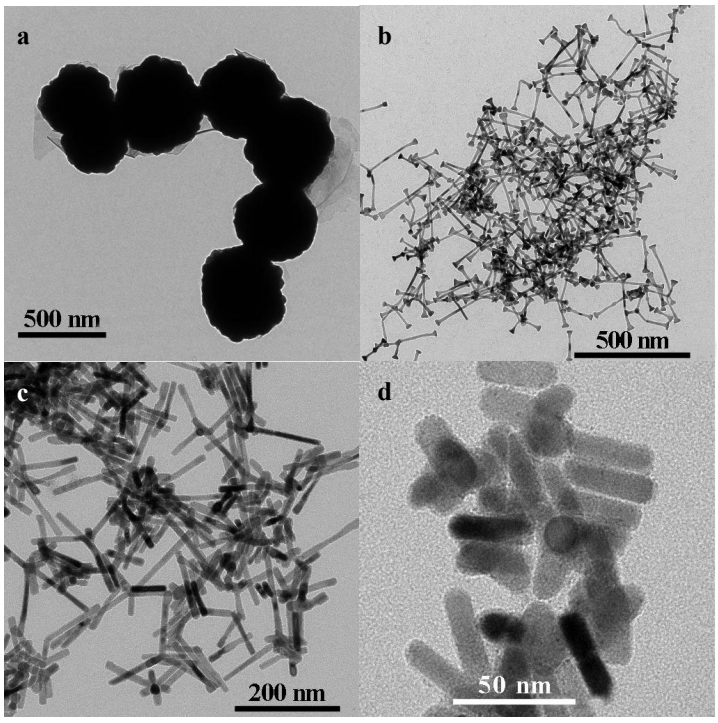

Figure 1. TEM images of cobalt nanomaterials synthesized with different Ir/Co molar ratios at 150 ℃: (a) 0 for 20 h and (b) 0.01, (c) 0.025 and (d) 0.05 for 10 h. The syntheses were kept under the conditions of 150 ℃, 0.2 g NaOH and 2.30 g sodium stearate.

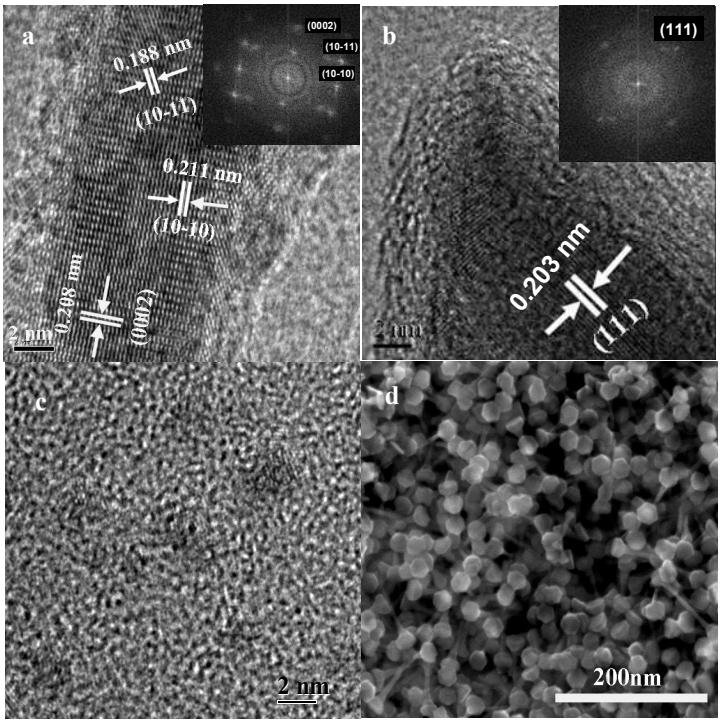

Figure 2. HRTEM images of cobalt nanorod (a), conical head (b), Ir nanoparticels (c) and conical heads by SEM image (d). Insets in (a) and (b) are the fast Fourier transform (FFT) patterns.

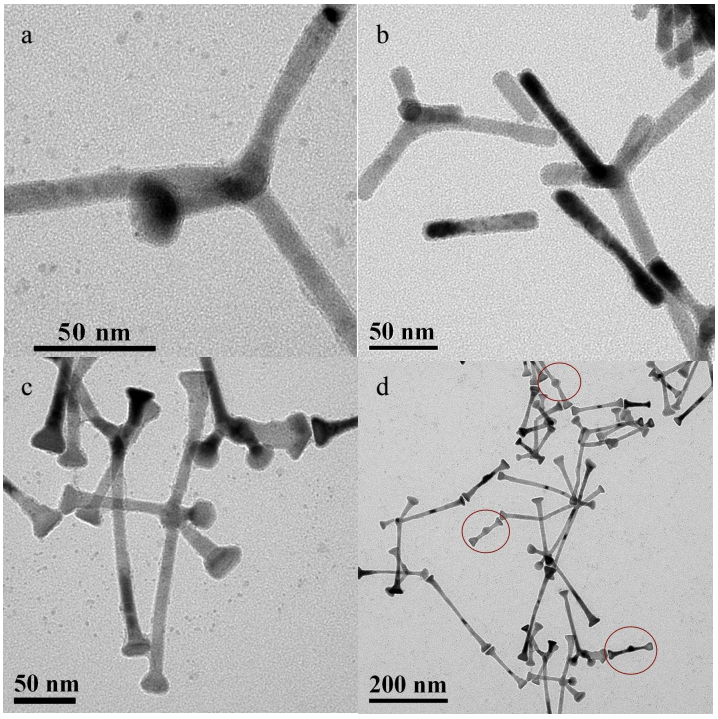

Figure 3. TEM images of cobalt multi-pods.

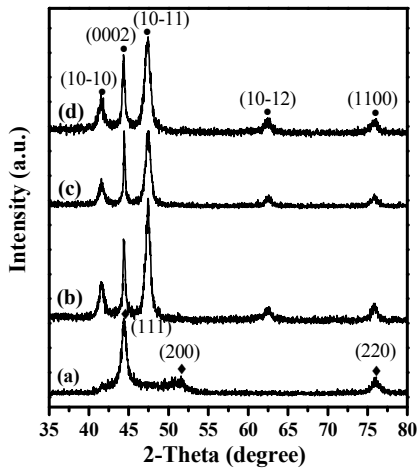

Figure 4. XRD patterns of cobalt nanomaterials synthesized with different Ir/Co molar ratios: (a) 0, (b) 0.01, (c) 0.025, and (d) 0.05. Entry (a) was conducted at 150 ℃ for 20 h. (●) and (◆) represent hcp and fcc phase, respectively.

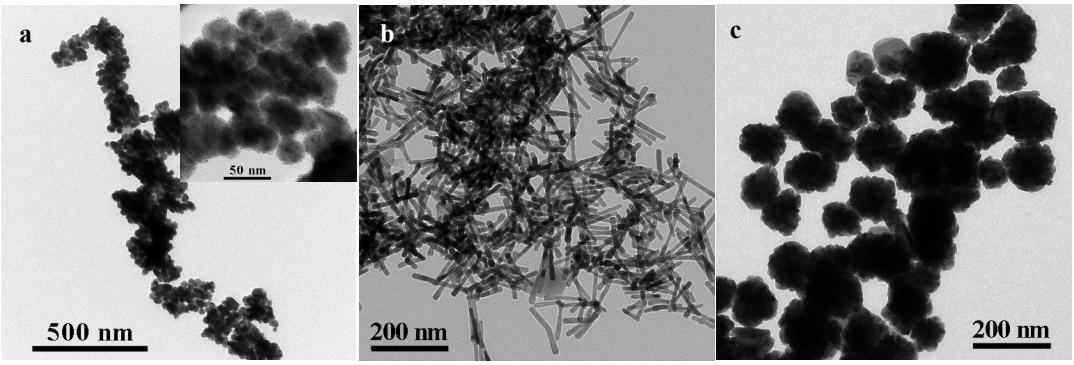

Figure 5. TEM images of cobalt nanomaterials synthesized with different NaOH amounts: (a) 0 g, (b) 0.2 g, and (c) 0.7 g. Synthetic condition: 2.30 g sodium stearate, Ir/Co= 0.025 (mol), 150 ℃, 10 h.

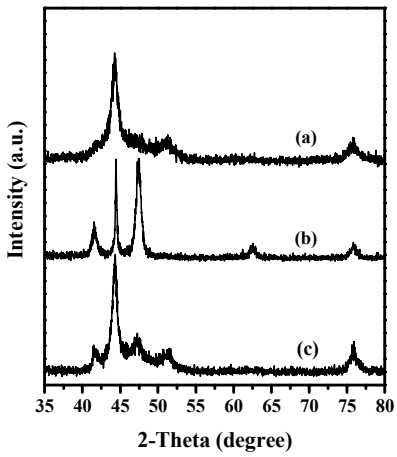

Figure 6. XRD patterns of cobalt nanomaterials synthesized with different NaOH amounts: (a) 0 g, (b) 0.2 g, and (c) 0.7 g.

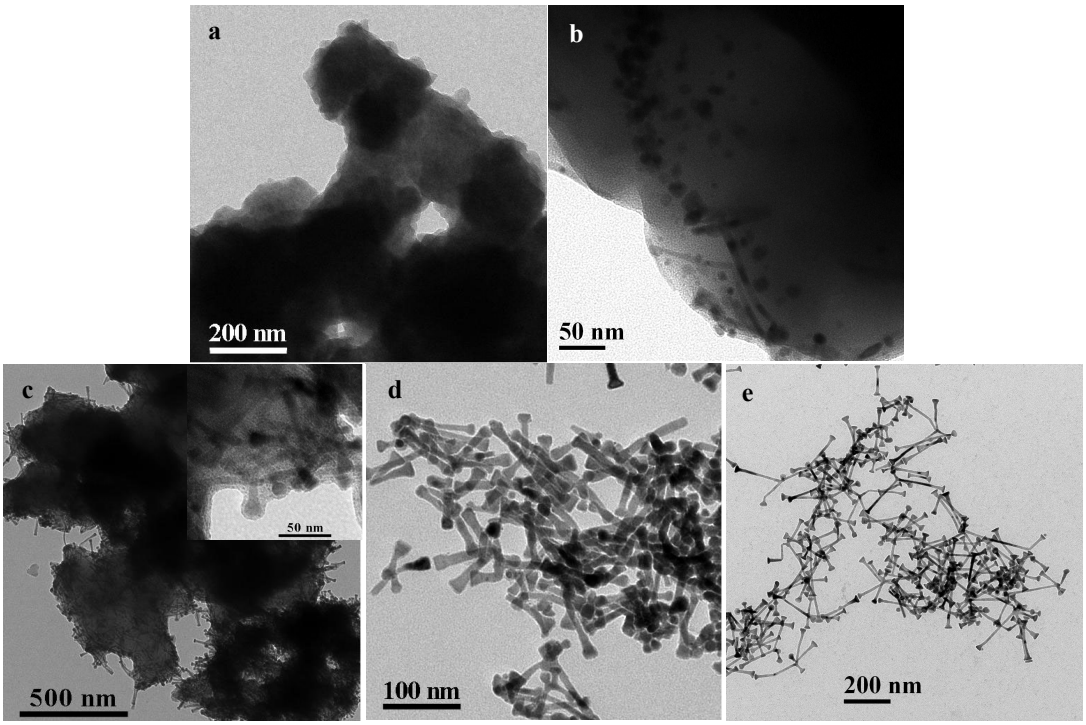

Figure 7. TEM images of cobalt nanomaterials synthesized at stages: (a) 0.5 h, (b) 1.0 h, (c) 1.5 h, (d) 3.5 h and (e) 10 h. Synthetic condition: 0.2 g NaOH, 2.30 g sodium stearate, Ir/Co=0.01 (mol), 150 ℃.

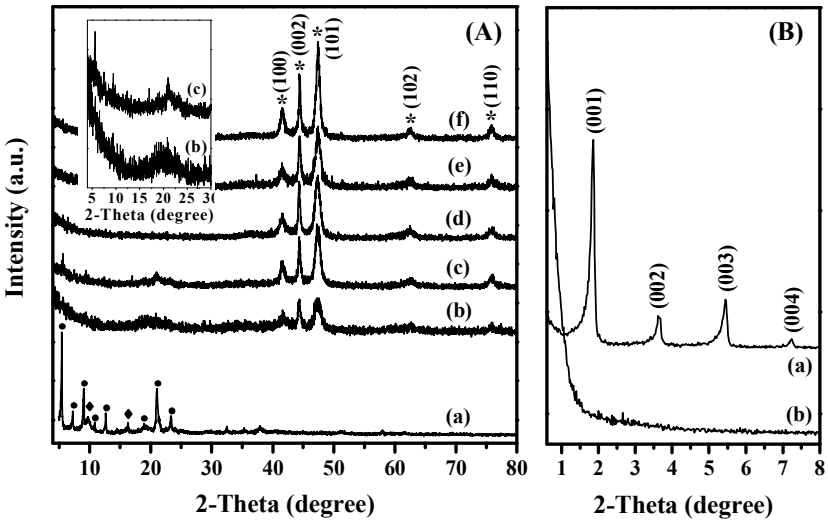

Figure 8. Wide (A) and low (B) angle XRD patterns of cobalt intermediates at different stages: (a) 0.5 h, (b) 1.5 h, (c) 2 h, (d) 3.5 h, (e) 6 h, and (f) 10 h. (*) represents metallic hcp cobalt, (●) and (◆) are the precursors cobalt stearate and cobalt alkoxide, respectively. Inset in (A) shows the magnified XRD pattern of (b) and (c) in the range of 4-30 °.

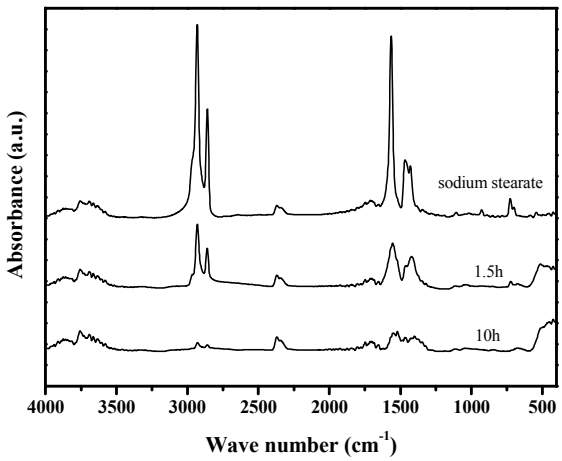

Figure 9. FT-IR spectra of cobalt nanorods synthesized at different stages.

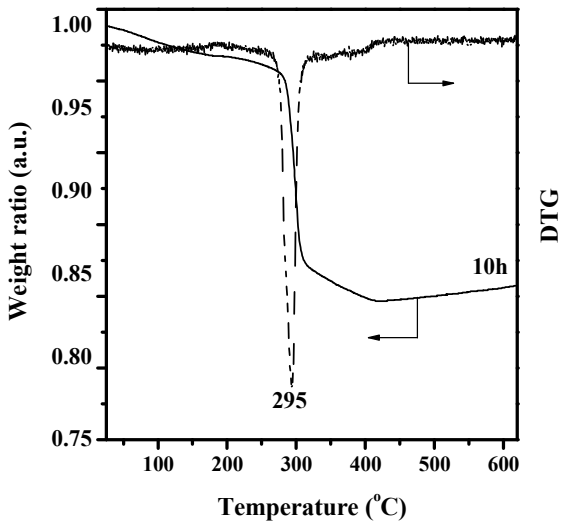

Figure 10. TG profile of cobalt nanorods. The rods were synthesized under the following conditions: Ir/Co=0.025 (mol), 2.30 g sodium stearate, 0.2 g NaOH, 150 ℃, 10 h.

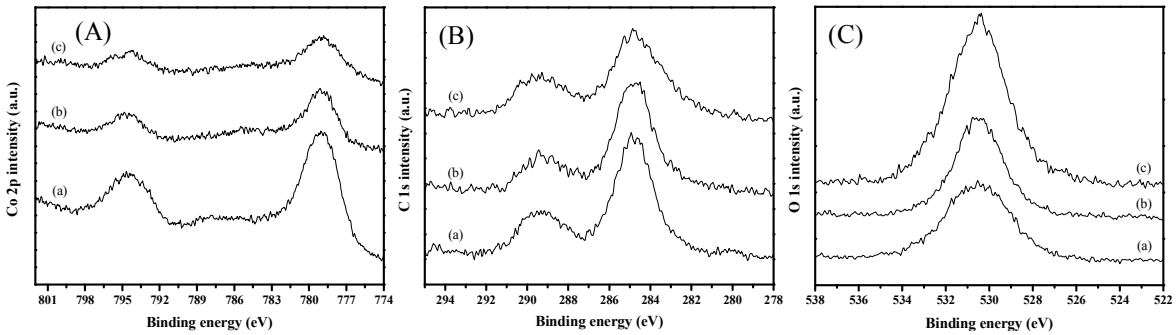

Figure 11. XPS spectra of cobalt nanorods with Co 2p core level (A), C 1s core level (B) and O 1s core level (C). (a), (b) and (c) represent the rods in Figure 1 (b), (c) and (d), respectively.

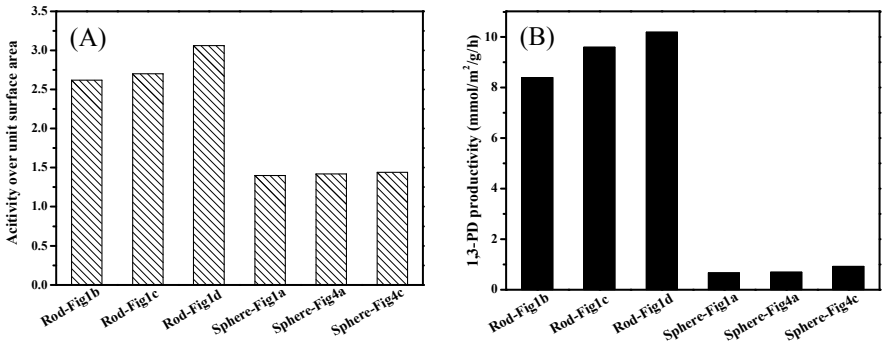

Figure 12. Glycerol conversion (A) and 1,3-propanediol productivity (B) on unit surface of cobalt nanomaterials.

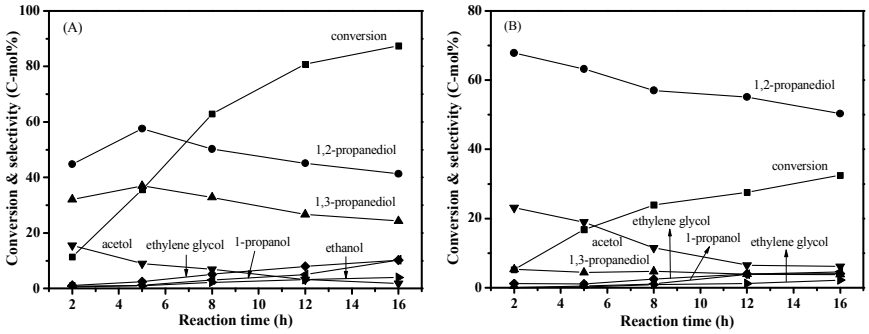

Figure 13. The influence of reaction time on glycerol hydrogenolysis over Co nanorods (A) and nanospheres (B).

Reaction conditions: catalyst, 0.06 g; temperature, 200; initial H_2 pressure, 3.0 MPa and 10% glycerol solution, 40 ml.

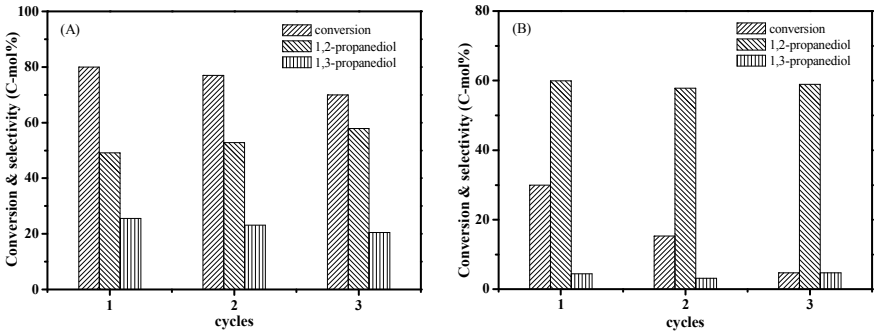

Figure 14. Catalytic stability of Co nanorods (A) and nanospheres (B) in glycerol hydrogenolysis. Reaction conditions: catalyst, 0.06 g; temperature, 200; reaction time, 12 h; initial H_2 pressure, 3.0 MPa and 10% glycerol solution, 40 ml.

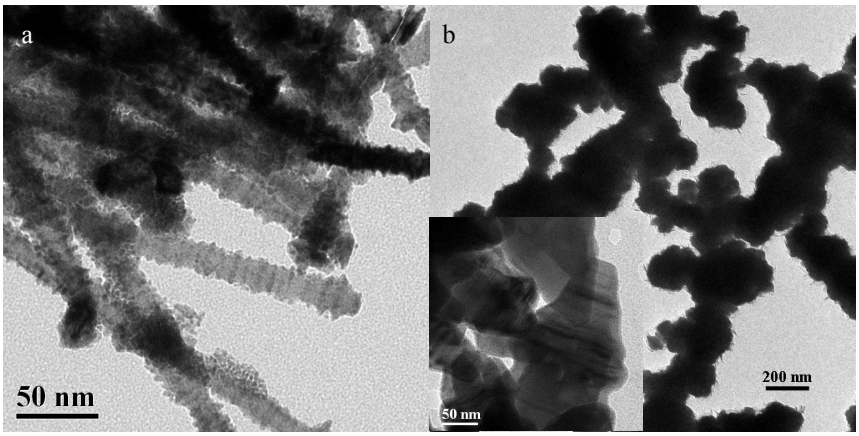

Figure 15. TEM images of cobalt nanorods (a) and nanospheres (b) after the third use in glycerol hydrogenolysis. The fresh rods and spheres were relative to Figure 1b and 5a, respectively.

Table 1. ICP-AES and BET results of cobalt nanomaterials

Sample	Ir/Co (mol, stoichiometry)	Ir/Co (mol, ICP)	Surface area (m^2/g, BET)
Co nanorods, Fig. 1b	0.01	0.0014	31.4
Co nanorods, Fig. 15a, reused	0.01	0.0011	35.7
Co nanorods, Fig. 1c	0.025	0.0028	26.9
Co nanorods, Fig. 1d	0.05	0.0029	20.2
Co nanospheres, Fig. 1a	-	-	1.5
Co nanospheres, Fig. 4a	0.025	0.0026	19.9
Co nanospheres, Fig. 15b, reused	0.025	0.0020	3.4
Co nanospheres, Fig. 4c	0.025	0.0021	5.3

Table 2. Hydrogenolysis of glycerol over cobalt nanomaterials [a]

Catalyst	Conversion (%)	Selectivity of products (C-mol %)						
		1,2-PD	1,3-PD	acetol	1-propanol	EG	ethanol	unidentified
Nanorods, Fig. 1b	82.4	48.0	23.1	4.8	4.4	7.3	3.3	9.2
Nanorods, Fig. 1c	72.6	41.1	25.5	5.1	5.3	3.5	2.9	16.6
Nanorods, Fig. 1d	61.9	47.2	24.2	4.6	3.1	3.4	2.2	15.3
Nanospheres, Fig. 1a	2.1	57.7	3.4	4.1	-	-	-	34.8
Nanospheres, Fig. 5a	28.3	55.9	3.5	5.8	4.1	4.4	1.9	24.4
Nanospheres, Fig. 5c	7.6	56.6	4.6	5.0	2.3	1.5	-	30.0

[a] Reaction condition: 10% glycerol aqueous solution, 40 ml; catalyst, 0.06 g; reaction temperature, 200 ℃; reaction time, 12 h; initial H_2 pressure, 3.0 MPa. PD, propanediol; EG, ethylene glycol.

Table of content

Metallic Co nanorods with controllable aspect ratio were fabricated by using Ir as heterogeneous agent. Comparing to Co nanospheres, the nanorods with mainly exposed {10-10} facets showed much higher activity and 1,3-propanediol selectivity in glycerol hydrogenolysis.

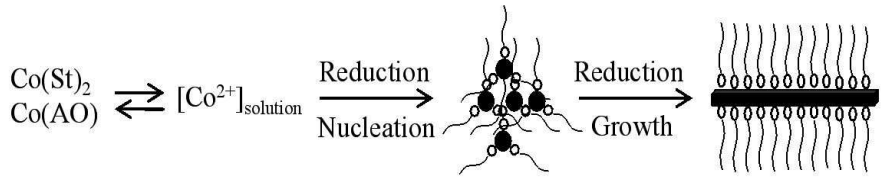

$Co(St)_2$: Cobalt stearate; Co(AO): Cobalt alkoxide